

DEVELOPMENT OF NANOMETER SCALE STRUCTURES IN COMPOSITES OF Nb-Ti AND THEIR EFFECT ON THE SUPERCONDUCTING CRITICAL CURRENT DENSITY

P. J. LEE and D. C. LARBALESTIER†

Applied Superconductivity Center, University of Wisconsin-Madison, Madison, WI 53706, U.S.A.

(Received 1 December 1986)

Abstract—A detailed investigation has been made of an optimized, high critical current density composite of Nb-46.5 wt% Ti. Details of the fabrication of the composite are given and an extensive metallurgical characterization of the microstructure at many stages in the fabrication and optimization process is presented. It is shown that up to 20% of α -Ti is produced by the heat treatment process. The mechanism by which the precipitate distribution is refined with increasing number of heat treatment and initially equiaxed precipitates turned into very thin, high aspect ratio ribbons by large drawing strains is quantitatively described. Critical current density measurements show that the optimum pinning forces are obtained for precipitates of ~ 1 nm in thickness, spaced ~ 4 nm apart. These dimensions are considerably smaller than those previously reported. There appears to be little or no proximity effect suppression of the pinning force even though the precipitate thickness is of order 0.2 coherence length. The specific pinning force of the precipitates ranges from 170 to 260 N/m², a value similar to that measured earlier for grain boundary film precipitation in this alloy.

Résumé—Nous avons étudié en détail un composite de niobium à 46,5% en poids de titane, composite à forte densité de courant critique. Nous donnons les détails de l'élaboration du composite et nous présentons une caractérisation métallurgique extensive de la microstructure à divers stades des procédures d'élaboration et d'optimisation. Nous montrons que le traitement thermique introduit jusqu'à 20% de Ti α . Nous décrivons quantitativement le mécanisme qui affine la répartition des précipités lorsque le nombre de traitements thermiques augmente, et qui transforme les précipités, initialement équiaxes, en rubans très minces grâce à de fortes déformations de tréfilage. Les mesures de densité de courant critique montrent que les forces d'épinglage optimales sont obtenues pour des précipités d'environ 1 nm d'épaisseur, espacés d'environ 4 nm. Ces dimensions sont très inférieures à celles qui ont été rapportées précédemment. Il semble qu'il y ait peu ou pas de suppression de la force d'épinglage par effet de proximité, même si l'épaisseur des précipités est de l'ordre de 0,2 fois la longueur de cohérence. La force d'épinglage spécifique des précipités varie entre 170 et 260 N/m², valeurs semblables celles mesurées antérieurement pour la précipitation de films intergranulaires dans cet alliage.

Zusammenfassung—Der optimierte Verbundwerkstoff Nb-46,5 Gew.-% Ti, der eine hohe kritische Stromdichte aufweist, wurde ausführlich untersucht. Die Einzelheiten der Herstellung werden dargelegt, außerdem wird die Mikrostruktur bei verschiedenen Stadien der Herstellung ausführlich metallurgisch charakterisiert. Bis zu 20% α -Ti entsteht während der Wärmebehandlung. Der Mechanismus wird quantitativ beschrieben, mit dem die Verteilung der Ausscheidungen mit zunehmender Anzahl der Wärmebehandlungen verfeinert wird, d.h. mit dem die anfangs gleichachsigen Ausscheidungen in dünne Bänder mit großem Seitenverhältnis durch die großen Dehnungen übergehen. Aus Messungen der kritischen Stromdichte ergibt sich, daß maximale Verankerungskräfte bei Ausscheidungen mit ungefähr 1 μ m Dicke, die im Abstand von etwa 4 nm liegen, erreicht werden. Diese Größen sind beträchtlich geringer als früher berichtete. Es scheint, daß trotz der Ausscheidungsstärke von etwa 0,2 der Kohärenzlänge keine oder nur eine geringe Unterdrückung der Verankerungskräfte durch den Proximityeffekt auftritt. Die spezifische Verankerungskraft der Ausscheidungen liegt zwischen 170 und 260 N/m²; dieser Wert ähnelt dem, der früher für die Korngrenzausscheidung in dieser Legierung gemessen wurde.

1. INTRODUCTION

Prior experiments on superconducting composites made from Nb-46.5 wt% Ti have shown that the flux pinning is very much enhanced by processing treatments which produce a very fine two phase microstructure. This was demonstrated by transmission electron microscopy (TEM) of longitudinal sections of commercial wires in which α -Ti could be clearly seen in the diffraction pattern although not readily

identified in bright field [1, 2]. Later work developed the techniques of transverse section preparation. Examination of both longitudinal and transverse sections is desirable when maximum information is required. Of the two, the transverse section is much more informative however. The reason for this is that the very extensive cold work given to these composites (the true strain, ϵ , generally exceeds 10) produces a strongly directional microstructure parallel to the drawing axis and this makes the microstructures considerably easier to interpret in transverse than in longitudinal section. The basic features

†Also Department of Metallurgical Engineering.

of the α -Ti precipitation process were determined in two studies of a commercially produced composite manufactured for the Fermilab Tevatron [3, 4].

A full evaluation of the significance of the microstructures observed in the Fermilab composite was compromised, however, by the considerable chemical inhomogeneities of the starting Nb-Ti alloy [4]. The ribbon morphology of α -Ti which corresponds to the optimum microstructure for flux pinning [5] was rather irregular and a quantitative analysis of the flux pinning could only be made for the grain boundary film morphology of precipitate. It was also observed that multiple heat treatments did not produce a significant beneficial effect on the critical current density (J_c) [3].

Prior work in our group had already raised concerns about the effect of local chemical inhomogeneities (of order ± 4 -5 wt%) in producing an irregular grain, sub-structure and precipitate morphology [6]. Following these experiments, W. K. McDonald and his group at Teledyne Wah Chang (TWCA) produced ingots of Nb-46.5 wt% Ti of much improved chemical homogeneity. These ingots ("High Homogeneity ingots") had local chemistry variations of only $\pm 1\frac{1}{2}$ -2 wt%. With them, we were easily able to raise the J_c by multiple heat treatments. For example, the prior inhomogeneous material did not respond effectively to multiple heat treatments and reached maximum J_c values of 1600-2000 A/mm² (5 T, 4.2 K, 10^{-14} Ω m). By employing 3-6 heat treatments on the High Homogeneity material, we were able to raise the J_c to 2800-3200 A/mm² [7].

A question raised by the TEM examination of the higher J_c composites concerns the mechanism of flux pinning and the practical limits to the J_c in these composites. It was observed that optimum J_c values were found for precipitates with thicknesses of 3-6 nm [5, 8]. These are extremely thin precipitates and they fall into a range where the mechanism of flux pinning is unclear. Since α -Ti is a non-superconducting phase, one would expect pinning of the fluxoid core by the precipitate to be important. However, the coherence length of Nb-46.5 wt% Ti is ~ 5 nm and the fluxoid diameter (~ 10 nm) is larger than the precipitate thickness. In the analysis of Kramer and Freyhardt [9], this would lead to a much reduced elementary pinning force because the proximity effect should induce superconductivity into such thin α -Ti particles. This view has been challenged by Matsushita [10] who came to the conclusion that there is no significant diminution of the elementary pinning force for thin precipitates. A study of ours on several commercial composites showed that the highest J_c values were found for the composites having the thickest precipitates. The data was too sparse to be conclusive, however, and no attempt was made to separate intrinsic from extrinsic factors in that study [8].

In all our previous studies described above, the only second phase to be conclusively identified was

α -Ti. More recently Hutchinson *et al.* [11] have reported the presence of ω phase in a composite fabricated from alloy of nominal composition Nb-46.5 wt% Ti. However, the processing details of the wire examined by these authors were not reported. A subsequent final size heat treatment of 167 h at 375°C produced only incomplete diffraction evidence for ω . Systematic work by Buckett and Larbalestier [12] has shown that increasing the strain at which a given heat treatment is given tends to suppress ω and favors the appearance of α -Ti. The ω phase was found to be suppressed at strains greater than about 4. It, therefore, appears that ω can be avoided by appropriate treatment of this alloy.

The present study was undertaken in order to clarify the precipitation modes in a "High Homogeneity" composite given multiple heat treatments which raised its J_c to very high values. A detailed superconducting critical current density characterization was also planned in order to attempt to clarify the relationship between the microstructure and the flux pinning.

2. EXPERIMENTAL DESIGN

2.1. Composite design and manufacture

In order to minimize uncertainties, as much of the fabrication as possible was performed in our laboratory. The Nb-Ti alloy was of "High Homogeneity" grade provided by Teledyne Wah Chang Albany (TWCA). Fabrication of the composite took place entirely in our laboratories. The rods of Nb-Ti were sheathed in OFHC copper and made into a 361 filament composite by a two stage stacking process.

Table 1 gives the location and details of the heat treatment and drawing schedule used. All heat treatments were for 10 h at 405°C. All drawing details are given in terms of the true strain ϵ ($= \ln A_0/A$) where A_0 is the cross-sectional area at the last Nb-Ti recrystallization. The rods used for our composite were supplied to us with a cold strain of 4.97, produced by mixed swaging and drawing [13]. No extrusion was used in fabricating the composite and hence there is no uncertainty about possible recovery effects of a warm working step at 550-650°C.

2.2. Metallographic examination

Samples were examined at various stages in the fabrication process using light microscopy (LM), scanning electron microscopy (SEM) and transmission electron (TEM) microscopy. A composition sensitive etch of equal parts lactic acid, H₂O₂, HNO₃ and HF developed by Paul Danielson of TWCA was used on specimens polished for light microscopy. Samples were prepared for examination by TEM using the jet electropolishing technique with a solution of 2 vol% HF, 5 vol% H₂SO₄ and 93 vol% methanol at -40°C and a polishing current of 1.8 mA mm⁻². Specimens used for energy dispersive X-ray microanalysis (EDS) were further thinned in a

Table 1. Heat treatment and drawing schedule

Number of filaments	Wire diameter (mm)	Nominal filament diameter (μm)	Nominal true strain	Heat treatment at this strain
1	—	3200	4.97	No
19	11.68	1960	6.00	Yes
19	6.63	1000	7.16	Yes
19	3.43	700	8.30	Yes
361	9.27	350	9.50	Yes
361	5.23	200	10.72	Yes
361	3.05	110	11.87	Yes
Final size wires				
361	0.927	30.6	14.25	No
361	0.813	26.8	14.52	No
361	0.721	23.8	14.76	No
361	0.622	20.5	15.05	No
361	0.572	18.9	15.22	No
361	0.508	16.8	15.45	No
361	0.477	14.7	15.72	No
361	0.404	13.3	15.91	No

Gatan Dual Ion Mill at 5 kV for 30 min, using a current of 0.5 mA in each gun. The transmission electron microscopy was carried out using a VG HB501 STEM, a JEOL 100B TEM, and a JEOL 200CX TEM/STEM at 100, 120 and 200 kV respectively. STEM EDS microanalysis was carried out using EDS facilities on the 200CX and HB501. Electron probe microanalysis (EPMA) was performed on metallographically polished bulk specimens, using an ARL EMX 30 microprobe at 20 kV.

The surface morphologies of the NbTi filaments were studied by chemical removal of the copper matrix with 1:1 HNO₃:H₂O, followed by examination in a JEOL 35C scanning electron microscope.

Quantitative measurements of length and area were made on 8" × 10" enlargements of the microstructure. Area measurements were made with a direct reading Numonics digitizer having a resolution of ±0.25 mm. Line lengths were measured with a calibrated wheel having a resolution of 0.5 mm.

2.3. Superconducting critical current measurements

All critical current (I_c) measurements were performed on ~0.6 m long samples mounted on copper and stainless steel barrels mounted co-axially inside the bore of a 12 T solenoid. The I_c was determined at an overall composite resistivity of 10⁻¹⁴ Ωm ($\approx 10 \mu\text{V/m}$). The resistive transition index n was determined from the slope of the log voltage-log current plot in the resistive transition, data being taken over the electric field range of about 10–40 $\mu\text{V/m}$.

The Cu:Nb-Ti ratio was determined by weighing the wire samples with and without the copper matrix, thus allowing conversion of I_c to J_c .

3. METALLOGRAPHIC RESULTS

3.1. Initial alloy state

The equiaxed grain morphology in the as recrystallized state is illustrated in Fig. 1. The ASTM grain size was determined to be 6.3, corresponding to

a mean lineal grain boundary intercept of 35 μm . The composition sensitive etch used for the specimens shown in Fig. 1(a) (transverse cross-section) and Fig. 1(b) (longitudinal cross-section) produced surface ripples, visible in these micrographs, corresponding to variations of about ±1.5 wt% Nb as measured by EPMA [see Fig. 2(a) and (b)]. Viewed in transverse cross-section by low magnification light microscopy or by flash radiography, the ripples form concentric circles about the center of the cross section and run parallel to the length of the billet in the longitudinal direction [Fig. 1(b)], forming a tree ring pattern. The chemical composition of rods of the alloy used for composite manufacture was determined by Teledyne Wah Chang Albany using standard wet chemical techniques and is given in Table 2. The Ti content was 47.8 wt% Ti and the O content 570 ppm. All values are typical for commercially produced Nb-46.5 wt% Ti.

The rods were examined at 3.2 mm diameter ($\epsilon = 4.97$) by TEM, and in general they were found to be homogeneous β -NbTi. In one specimen some isolated α -Ti precipitates were discovered at grain boundaries. The α -Ti precipitates ranged in length from 150 to 500 nm and were less than 50 nm in width. The volume fraction of precipitate was esti-

Table 2. Wet chemistry results on 3.2 mm diameter rod used for this study

Element	Content (ppm)
Al	32
C	70
Cr	<50
Cu	<10
Fe	72
H	20
Mg	<25
N	40
Ni	<25
O	570
Si	<100
Sn	<40
Ta	480
Ti (wt%)	47.8

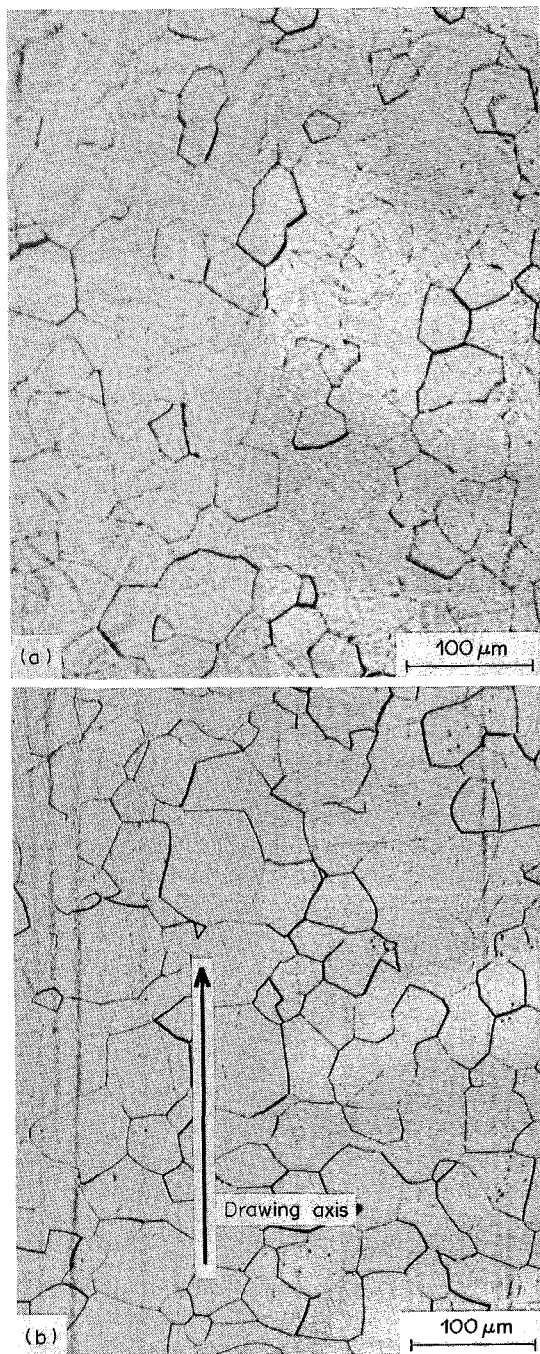
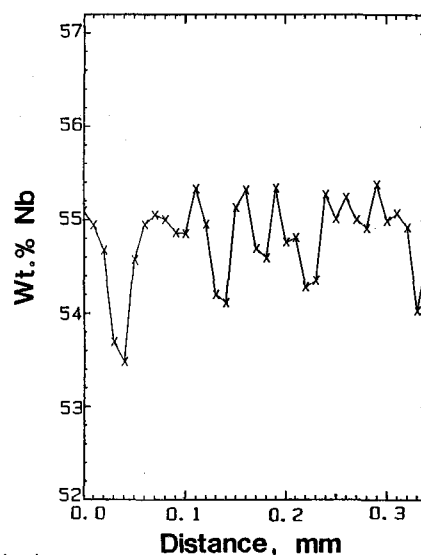


Fig. 1. Light micrograph of Nb-Ti ingot after final recrystallization anneal (a) in transverse cross-section, (b) in longitudinal cross-section. The cross-sections have been given a composition sensitive etch.

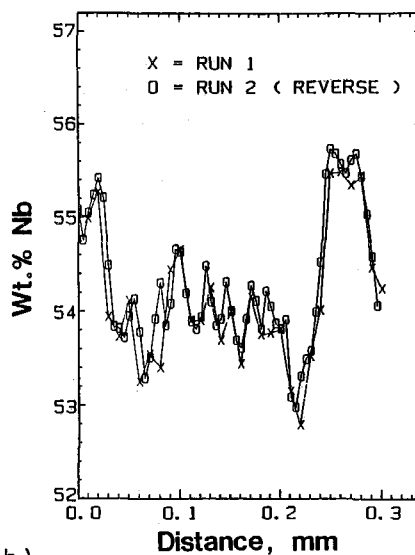
mated at less than 2%. No other second phases were found.

3.2. Microstructures produced by the optimization heat treatments

The first heat treatment at $\epsilon = 6.00$ caused precipitation of α -Ti (confirmed by selected area electron diffraction and EDS) at grain boundary triple points. Figure 3(a) is a STEM Nb L_{α} X-ray map of a



(a)



(b)

Fig. 2. Radial point traverse by EPMA of Nb-Ti ingot after final recrystallization anneal (a) near the center, (b) near the edge of the billet.

transverse cross-section at this stage. The α -Ti precipitates appear as dark regions due to their very low Nb concentration. Microanalysis of the α -Ti precipitates, Fig. 3(b), gave a composition of approximately 5 at.% Nb. The possible excitation of surrounding Nb-Ti matrix, however, may have contributed to the measured intensities and thus exaggerated the Nb content of the precipitates.

In addition to the triple point precipitates, the heat treatment produced a thin (< 4 nm) grain boundary film. The film was produced at all high angle grain boundaries and in these cases was uniform in thickness and continuous. The film was also produced at

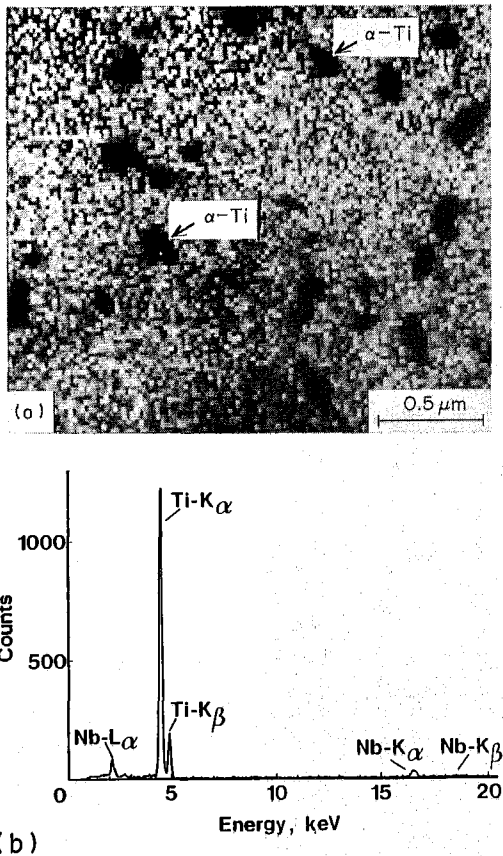


Fig. 3. (a) STEM/EDS Nb-L α X-ray map of transverse cross-section of Nb-Ti filament after 1st heat treatment (two representative α -Ti precipitates are indicated) (b) EDS spectrum from α -Ti precipitate, taken at 200 kV, after 1st heat treatment.

low angle boundaries but in these cases was neither uniform nor continuous.

The transverse section cross-sectional areas of the precipitates were measured by planimetry so that the effect of cold work and heat treatment on the precipitate size and distribution could be monitored. About 9% of the cross-sectional area of the filament was α -Ti after the first heat treatment, as is shown in Table 3.

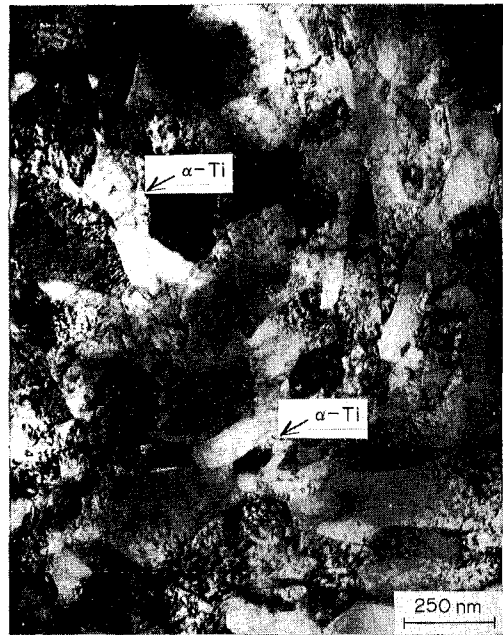


Fig. 4. TEM image of transverse cross-section of Nb-Ti filament prior to 2nd heat treatment (tilted 4° from β <110> axis), two representative α -Ti precipitates are indicated.

After a further drawing strain of 1.16 ($\epsilon = 7.16$) the grain morphology in the transverse cross-section, approximately equiaxed after the first heat treatment, became more distorted, Fig. 4. Accompanying this strain there was a 60% reduction in the cross sectional area of the precipitates (as observed in transverse section), roughly equivalent to the reduction in the cross-sectional area of the filament.

A second heat treatment resulted in a return to the equiaxed transverse cross-sectional microstructure and a coarsening of the precipitates. Continued drawing and subsequent heat treatment cycles gradually refined the precipitate size and distribution. Figures 5(a) and (b) compare the microstructures after the first ($\epsilon = 6.00$) and fourth ($\epsilon = 9.50$) heat treatments and illustrate the great refinement in the microstructure which has been produced by three additional heat treatment and draw cycles. The volume

Table 3. Results of planimetry measurements on precipitation of α -Ti during thermomechanical processing

Nominal true strain	Nominal filament diameter (μm)	Heat treatments	Vol.% α -precipitate	Mean transverse cross-sectional area of α -precipitates (nm^2)	Equivalent round diameter ^c (nm)
6.00	1960	1	9	11,000	120
7.16	1000	1 ^a	6	4600	77
7.16	1000	2	8	6200	89
9.50	350	4	17	6900	94
10.72	200	4 ^b	16	2600	58
10.72	200	5	21	4800	78
11.87	110	6	17	6000	87

^aBefore 2nd H.T.

^bBefore 5th H.T.

^cWhere equivalent round diameter = $\sqrt{\frac{4}{\pi} \cdot \bar{A}}$.

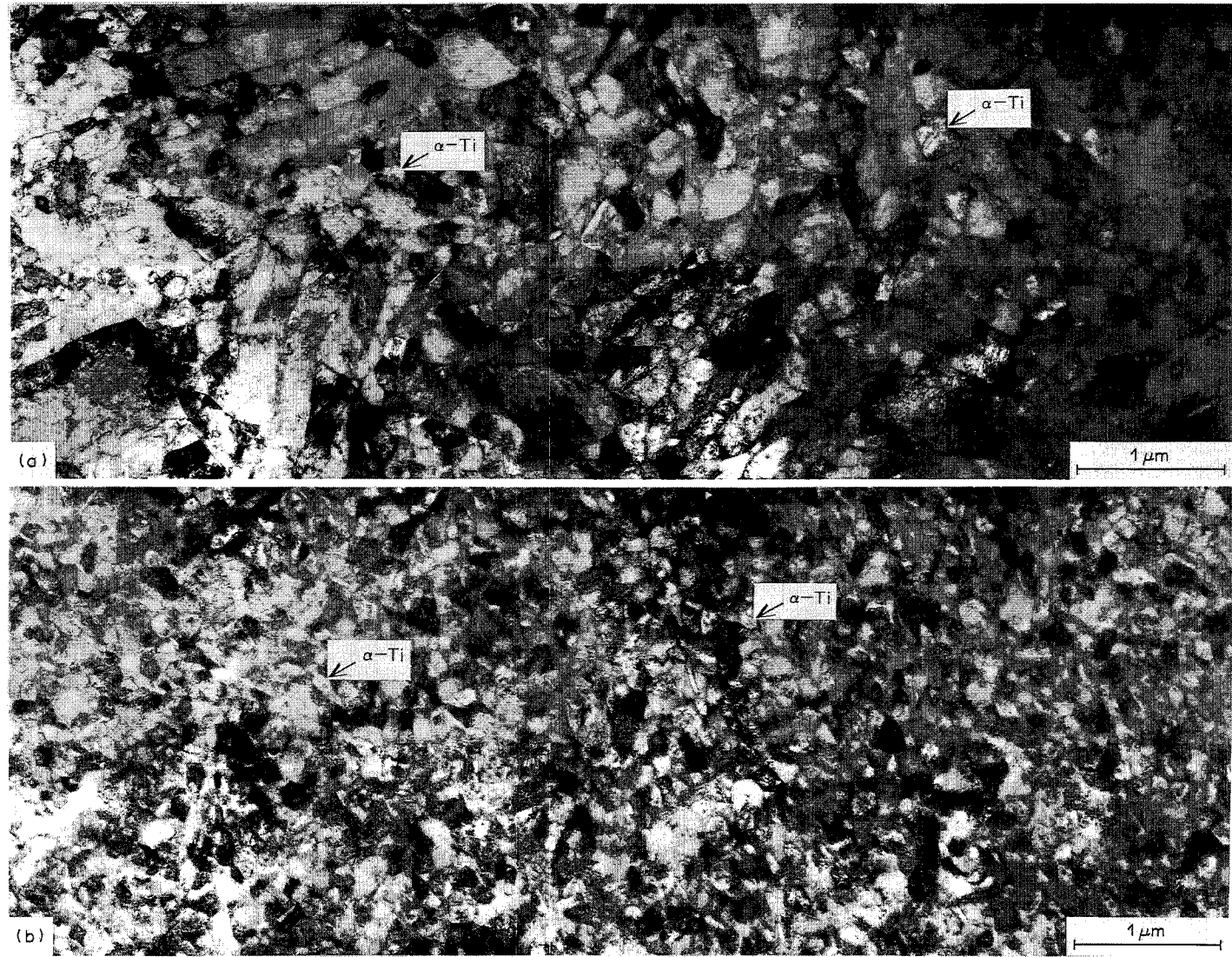


Fig. 5. Low magnification bright field TEM image of transverse cross-section of Nb-Ti filament (a) after 1st heat treatment (tilted 5° from $\beta\langle 110 \rangle$ axis), (b) after 4th heat treatment (tilted 4° from $\beta\langle 110 \rangle$ axis). Two representative α -Ti precipitates are indicated for each micrograph.

fraction of α -Ti increased from 6 to 9% (first HT) to 16% (fourth HT) while the average precipitate cross-section declined from 11,000 to 6,900 nm². The precipitate size diminished particularly strongly following the first heat treatment. The selected area diffraction patterns indicated a fairly uniform distribution of grain orientations around the $\langle 110 \rangle_{\beta}$ drawing direction.

After the sixth ($\epsilon = 11.87$) and final heat treatment, the mean cross-sectional area of the α -Ti precipitates had fallen to 6000 nm² and the precipitates were found to be uniformly distributed across the filament. The considerable difference between the microstructures of the transverse and longitudinal cross-sections is illustrated in Figs 6(a) and (b), where transverse and longitudinal sections after the final heat treatment are compared. The α -Ti precipitates in the TEM foil shown in Fig. 6(a) are thicker in the beam direction than the surrounding β -Nb-Ti matrix, due to a slower polishing rate. In this case the α -Ti appears darker than the β -Nb-Ti, except at the precipitate edges, which are of comparable thickness to the matrix. The edges thus appear lighter, as explained above.

The pattern of α -Ti precipitate growth during thermomechanical processing should be noted. Figures 5(a) and (b) illustrate the growth in precipitate size relative to the Nb-Ti grain size between the first and fourth heat treatment. Examination of Table 3 reveals that the α -Ti precipitate size after heat treatment remained approximately constant for all heat treatments beyond the second, despite the reduction in β -Nb-Ti grain size produced by each strain increment (e.g. see Fig. 5). The volume fraction of precipitate appeared to increase markedly between the second and fourth heat treatment (unfortunately no sample was available for the third heat treatment), reaching an approximately constant value (17–21%) after the fourth heat treatment.

3.3. Final size microstructures

Between the final heat treatment and the first final size wire examined, the composite received an additional strain of 2.38. The microstructure of the final size wires differed markedly from that previously observed. The α -Ti precipitates were drawn into highly aspected thin ribbons that were, on average, less than 2 nm thick. An attempt was made to quantify the thickness and separation of the ribbons. However, many precipitates were less than 1 nm thick, making their accurate and consistent measurement difficult. The measurements of linear intercept were all made on transverse cross-sections, at a magnification of 420,000 over distances of between 0.5 and 1 μ m within the filament. The ribbon thickness at the point of intersection was measured, rather than the length of line crossing the precipitate since this is believed to be more appropriate for explaining the flux-pinning behavior.

Some care was needed in order to obtain micro-

graphs suitable for quantitative measurement. Since the α -Ti ribbons become visible primarily due to their greater electron transmission efficiency and since they were aligned parallel to the wire drawing axis, it was necessary to have the electron beam parallel to the wire axis in order to view all ribbon orientations. If this was not the case, a preferred orientation of ribbon was observed and only those ribbons whose axis was close to the beam axis were found to be visible. However, the marked $\langle 110 \rangle_{\beta}$ drawing texture of the filament produced strong diffraction contrast when the beam was exactly parallel to the wire axis. Hence it was found advantageous to produce micrographs just off the axis, sometimes at several different

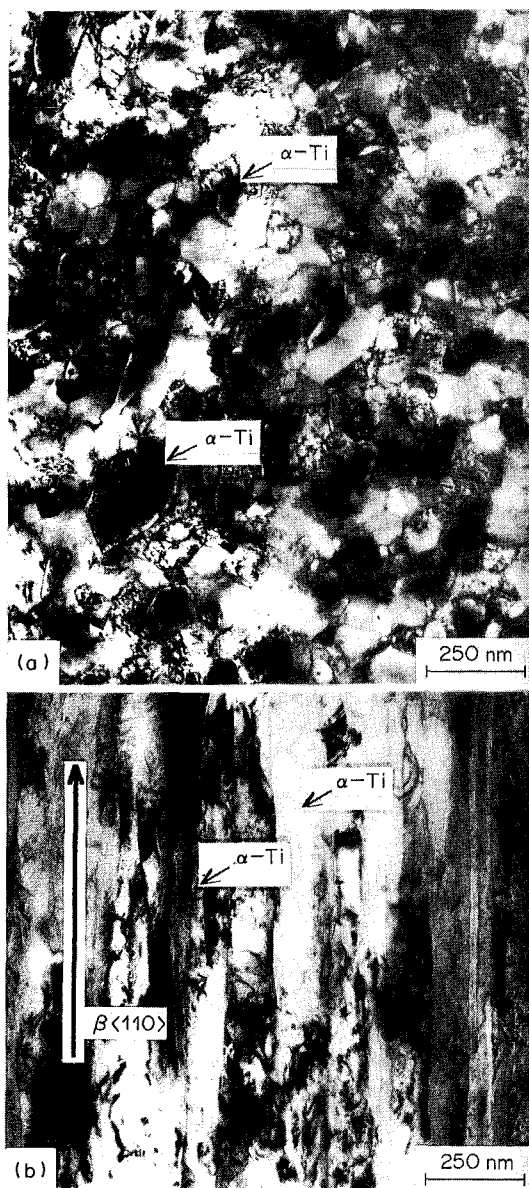


Fig. 6. TEM image of Nb-Ti filament after 6th heat treatment (a) in transverse cross-section (tilted 6° from $\beta \langle 110 \rangle$ axis), (b) in longitudinal cross-section. Two representative α -Ti precipitates are indicated.

Table 4. α -Ti Ribbon measurements

Wire diameter (mm)	Final drawing strain, ϵ_f	Average ribbon thickness (nm)	Ribbon density length/area (Mm/m ²)	$F_{p,max}(5T)$ (GNm ⁻¹)	Q_{ppt} (Nm ⁻²)
0.927	2.38	2.14	99	12.96	260
0.813	2.65	1.70	—	—	—
0.721	2.89	1.77	125	14.04	224
0.622	3.18	0.98	—	—	—
0.572	3.35	0.97	174	14.81	170
0.508	3.58	0.92	—	—	—
0.447	3.85	0.99	130	12.87	197
0.404	4.04	0.98	—	—	—

orientations, in order to check that as many ribbons as possible were observed. In some cases it was not found possible to avoid some directionality of the ribbons in the micrographs. In these cases, the orientation of the linear intercepts was chosen so that the intercepts were normal to the perceived ribbon alignment, since these ribbons were at optimum contrast.

The results of these measurements are given in Table 4. The mean thickness varied from ~ 2 nm at the largest wire size, leveling off at ~ 1 nm at the smaller sizes. We believe that this leveling off is probably an artifact of the measuring process. Features smaller than 0.7 nm could not be reliably interpreted and a measurement limit was set at this value. The thickness measurements given in Table 4 tend towards the measurement limit at the finer wire sizes, suggesting that the true ribbon thickness falls below these values. The total volume of precipitate measured remained constant at about 20%. The mean ribbon separation could thus be estimated by multiplying the ribbon thickness by four. At the optimum wire size (i.e. that with maximum J_c), the average measured ribbon thickness was only 1 nm and the ribbon separation 4 nm. At this wire size only 9% of

the ribbons measured had a thickness greater than 1.5 nm and no ribbons were found thicker than 8.5 nm. The majority of ribbons in this case had a thickness less than 1 nm. For all the wires examined, the majority of ribbons were less than 1.5 nm thick and there were no ribbons thicker than 10 nm.

The typical folded ribbon microstructure of an optimized conductor is shown in Fig. 7 for a 0.57 mm diameter wire. In Fig. 8, a longitudinal section of a 0.62 mm diameter wire is shown, in which α -Ti ribbons can be seen running parallel to the drawing axis. The ribbons were often 1–2 μ m long.

3.4. Filament–matrix reactions

SEM micrographs of a filament surface and of a number of filaments at the 0.62 mm wire size are shown in Fig. 9(a) and (b) respectively. The surfaces of the filaments are seen to be studded with intermetallic nodules. STEM-EDS studies indicated that the nodules were formed by a reaction between the Cu matrix and the Ti in the superconductor [14, 15]. The intermetallic is not a continuous layer but is limited to the discrete nodules shown in Fig. 9. It is

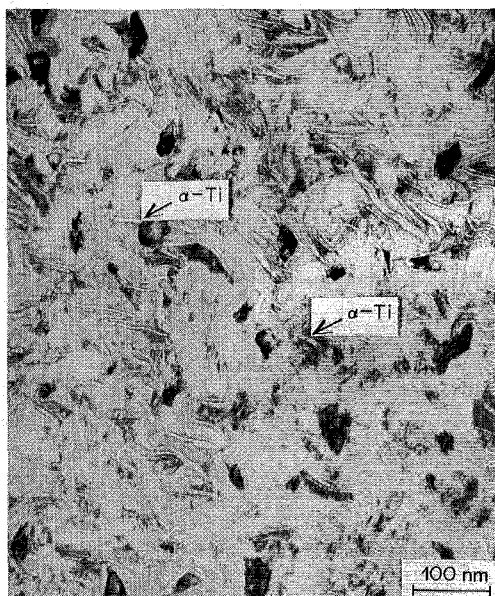


Fig. 7. TEM image of transverse cross-section of Nb-Ti filament at 0.572 mm wire diameter (tilted 4° from β $\langle 110 \rangle$ axis). Two representative α -Ti ribbons are indicated.

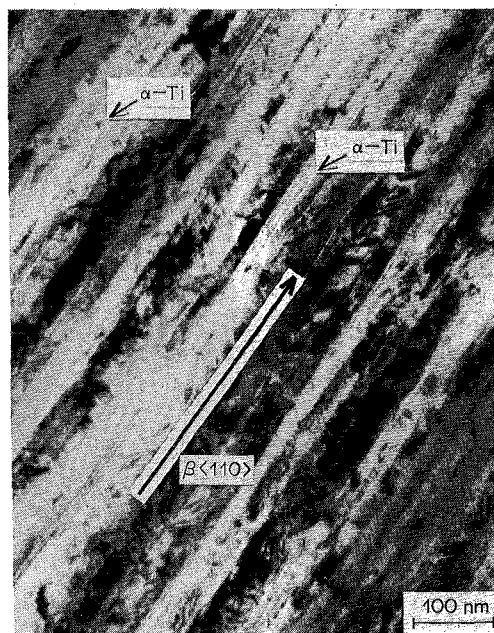


Fig. 8. TEM image of longitudinal cross-section of Nb-Ti filament at 0.622 mm diameter. Two representative α -Ti are indicated.



Fig. 9. (a) SEM image of several Nb-Ti filaments from 0.622 mm wire after acid removal of Cu matrix, (b) SEM image of filament surface from 0.622 mm wire.

believed that the formation of these brittle intermetallics results in inhomogeneous drawing properties. Measurements were made on the cross-sectional areas of the 19 filaments in the center bundle of each wire in order to assess the filament uniformity, and these results are shown in Fig. 10. The plot of standard deviation in filament cross-section, expressed as a percentage of the mean filament cross-sectional area, versus wire diameter indicates a considerable deterioration in filament uniformity with increasing final drawing strain. The distribution of wire sizes appears to change from an approximately normal distribution at the larger wire sizes to a bimodal distribution at the finest wire. This suggests that a sympathetic sausageing of the filaments occurred.

4. SUPERCONDUCTING PROPERTY RESULTS

4.1. Critical current densities

Critical current densities at 3, 5 and 8 T for wires ranging in size from 0.927 to 0.404 mm are shown in

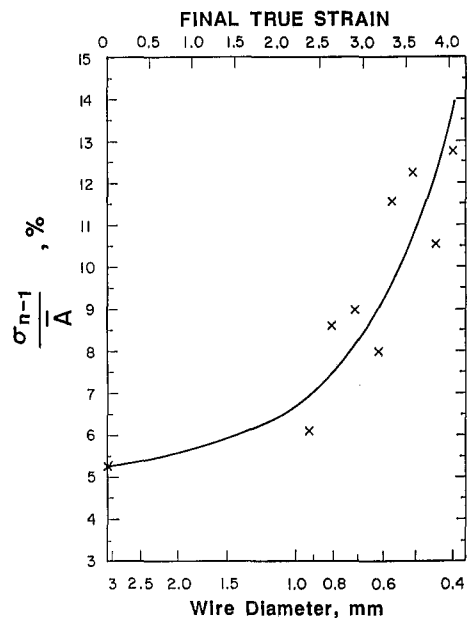


Fig. 10. Variation in uniformity of filament cross-sectional area with final drawing strain and wire diameter.

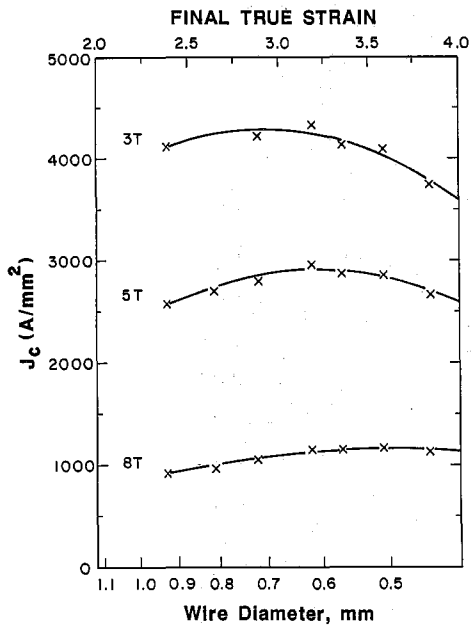


Fig. 11. Variation in J_c (4.2 K, $10^{-14} \Omega m$) with final drawing strain and wire diameter.

Fig. 11. These sizes correspond to total drawing strains since the last recrystallization of the Nb-Ti of 14.25 to 15.91, the final drawing strain (ϵ_f) since the 6th heat treatment ranging from 2.38 to 4.04. The wires were drawn to size without breakage problems.

The data of Fig. 11 show that increasing ϵ_f initially raised the J_c at all fields. However, when ϵ_f exceeded about 3–3.5, the J_c was found to peak. This peak occurs earlier at lower fields (e.g. at $\epsilon_f = 3.18$ (0.62 mm dia) at 3 T and 5 T but at $\epsilon_f = 3.58$ (0.508 mm dia) at 8 T). The fall off in J_c at low fields is particularly marked for the higher strains and a distinct change in the shape of the pinning force curves is observed (Fig. 12). The effect of strain on the high field J_c and pinning force are small by comparison. Beyond the optimum strain for the mid-field J_c , J_c (8 T) changes by less than 4%.

Figure 13 plots the resistive transition index for the different sized wires. Although there is some scatter in the individual values, the trend of the plots is quite clear. At large size (e.g. 0.927 mm) the plot is steeply increasing with decreasing field, n (5 T) reaching about 70. At the smallest size (0.404 mm) the plot became rather independent of field below about 8 T. In this case, n (5 T) fell to about 30.

5. DISCUSSION

5.1. Quantitative metallography

A vital component of any quantitative description of the superconducting properties is a quantitative description of the microstructure. We believe that the present work is a major step towards providing such

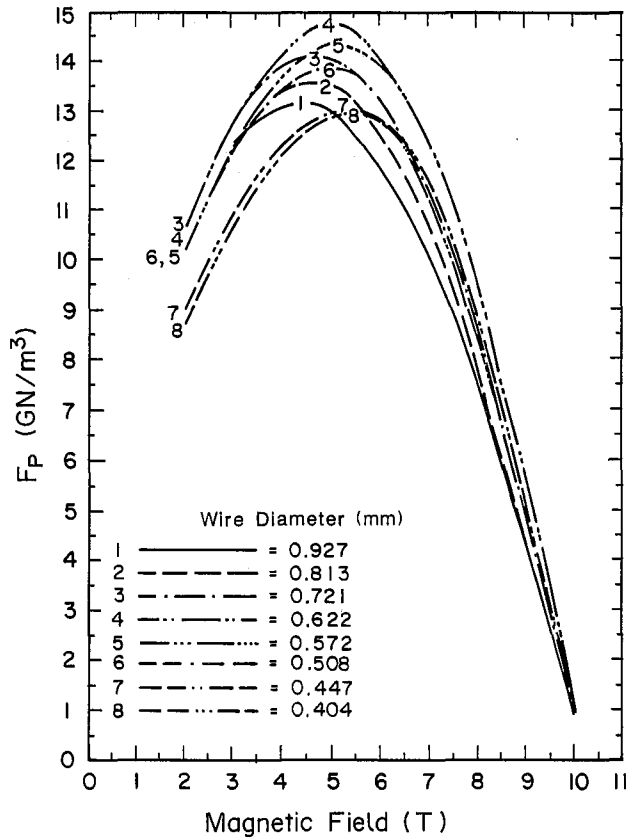


Fig. 12. Variation of flux pinning behavior with applied field for all wire sizes.

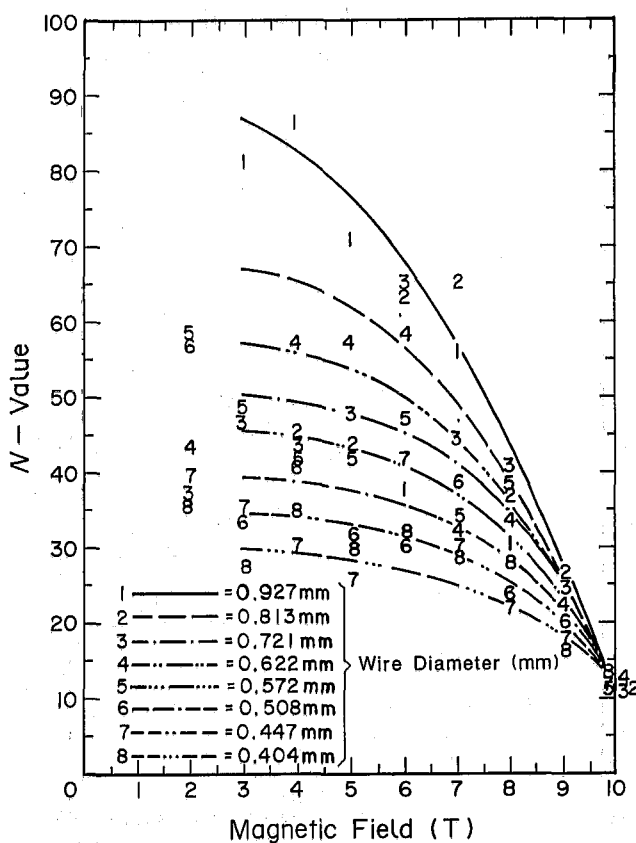


Fig. 13. Variation in resistive transition index with applied field for all wire sizes.

a description for the optimized microstructure characteristic of very high J_c Nb-Ti composites.

The results obtained show that the volume percentage of α -Ti increases with increasing number of heat treatments, reaching a maximum value of 17–21% after the fourth heat treatment. The origin of the variation of this value is not clear. Some of it is presumably due to statistical variation in the foils examined, while some of it may come from the incorrect assumption that the volume fraction is exactly equivalent to the measured cross-sectional area fraction. We did not examine longitudinal sections of all foils and could not, therefore, check for changes in precipitate aspect ratio which might modify the above assumptions. The values of 17–24% obtained are broadly consistent with earlier measurements in our group on commercially optimized composites (of unknown processing) in which $\sim 15\%$ α -Ti was seen [5]. Within the limit of resolution of the EDS technique, the composition of Nb in the α -Ti was seen to be consistent with the published phase diagram, [16], i.e. Ti 5 at.% Nb.

The quantitative analysis of the α -Ti ribbon microstructure is not without some uncertainties. A lower measurement limit of 0.7 nm was established, this being the minimum thickness which could consistently be identified on the micrographs. The pre-

cautions taken to identify all orientations of the precipitates have already been discussed (Section 3). Figure 14 plots the mean ribbon thickness and the J_c (5 T) versus wire diameter. For the larger wires there is an approximate proportionality but below about 0.62 mm wire diameter, the mean measured ribbon thickness levels off at a value of ~ 1 nm. We believe that this leveling is apparent and not real. It arises because we could not consistently observe ribbons thinner than 0.7 nm. It should be noted that this limit is only about twice the lattice parameter of α -Ti ($c = 0.47$ nm, $a = 0.30$ nm). We offer as a reasonable, but unproven, hypothesis the interpretation that the ribbons continue to diminish in thickness below the limit at which we can observe them, finally dissolving into the matrix as the deformation continues.

The evidence of the micrographs in the present study does show how very ductile α -Ti precipitates are, even at the high densities and small separations observed in the smallest wires. The composites too are exceptionally ductile. The total strain since the last anneal of the Nb-Ti was about 16 for the finest wire tested and we observed no brittleness of the composite. Precipitate separation was as little as 4 nm and the α -Ti precipitates themselves deformed from diameters of ~ 50 –100 nm to very highly aspected ribbons < 1 nm thick with no apparent brittleness.

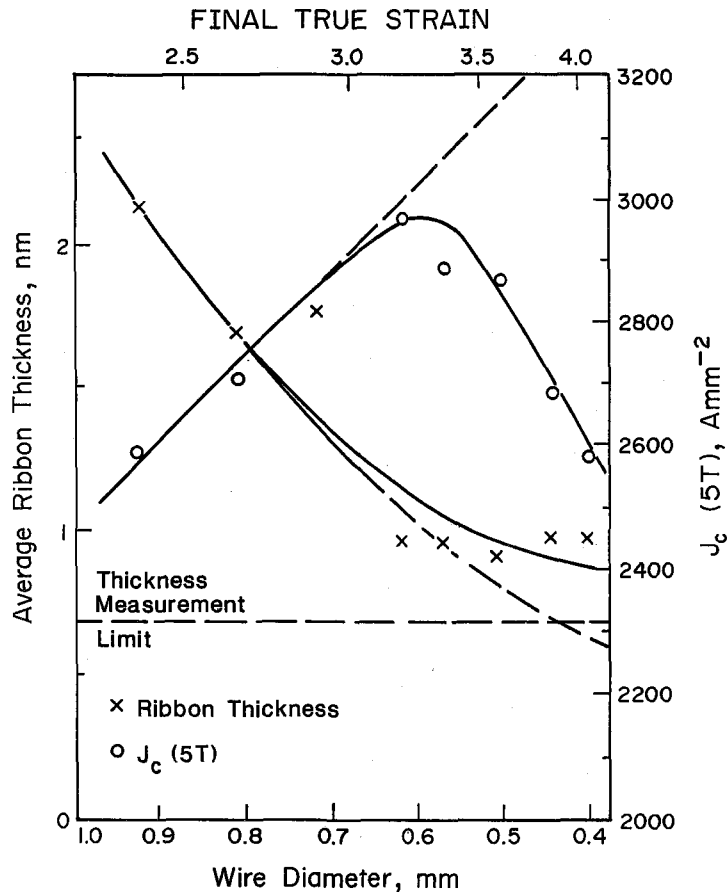


Fig. 14. Variation in J_c (5 T, $10^{-14} \Omega m$) and α -Ti ribbon thickness with final drawing strain and wire diameter.

This suggests that earlier interpretations which proposed that α -Ti precipitates were broken up by drawing are incorrect [17].

One final point can be raised here. The exceptional thinness of the ribbons in the optimized wires suggests that the presence of artefacts should be considered. For example, Fresnel fringes of similar contrast to the ribbons can be produced by amorphous grain-boundary films, by small gaps between grains and by a structured grain boundary [18]. However, ribbons were never seen in samples which had not been heat treated. A second check was also made. The proportion of α -Ti precipitates as measured by the ribbon cross-sections was compared to the measurements of α -Ti at heat treatment size. The agreement was always rather close.

5.2. Relationship between microstructural and superconducting properties

The basic issue raised by the present results is shown in Fig. 14. This figure shows that the J_c continues to increase as the precipitate thickness is reduced, the maximum transport J_c in the present case being obtained for the 0.622 mm diameter wire in which the mean ribbon thickness was 1 nm. It should be noted that this corresponds to a mean

precipitate spacing of ~ 4 nm. Since the coherence length (ξ) for Nb-46.5 wt% Ti is ~ 5 nm, the fluxoid diameter is ~ 10 nm. Given the established ideas of fluxoid core pinning by normal precipitates, we would expect these precipitates to be a long way below the optimum in size. Any given fluxoid will thus intersect two or three precipitates simultaneously across its width; the local free energy of the fluxoid should be rather insensitive to small displacements even when the long dimension (in transverse section) of the precipitate is parallel to the fluxoid axis. This situation might be expected, therefore, to yield only a small elementary pinning force (f_p).

The basic problem of determining the elementary pinning force from our measurements (which give the bulk pinning force F_p) remains. As we have previously described [4], we expect the elementary pinning force of the precipitates at heat treatment size to be large, since the precipitate diameter is approximately ten times the coherence length. However the density of fluxoid-precipitate interactions is then relatively low and the bulk pinning force should be small. Drawing the wire after heat treatment decreases the precipitate separation, thus increasing the density of interactions and raising F_p . This is indeed what is normally seen and is confirmed in Fig. 14. At

some point, however, the thickness of the precipitates might be expected to diminish to such an extent that f_p would significantly decline. The peak in the bulk pinning force F_p should then be a balance between an increasing density of pinning interactions and a weakening elementary pinning force. The surprising aspect of the present results is that the optimum bulk pinning force occurs for precipitate dimensions which are so small relative to the coherence length.

In a previous paper [4] we evaluated the grain boundary pinning force of 46.5 wt% Ti composites given only a final size heat treatment. Using Kramer's [19] formalism, the specific boundary pinning force (Q_{GB}) was calculated from

$$Q_{GB} = F_p / \lambda S_{GB}$$

where S_{GB} is the area of grain boundary per unit volume and λ an efficiency factor which accounts for the proportion of grain boundary oriented for pinning. This factor is not at all well-known. The figure previously used for columnar grains is 0.5 [4, 20]. Using this approach, grain boundary pinning forces (5 T, 4.2 K) of ~ 90 N/m² (single phase alloy) and ~ 300 N/m² (boundaries decorated by a 2–3 nm thick Ti-rich film) were derived.

In the past we have not found it possible to unambiguously identify the grain boundary film. [3, 4]. The similarity of the thickness of the grain boundary film and the optimized α -Ti ribbons suggests a comparison of the specific pinning forces. Table 4 collects the various microstructural measurements and F_p (5 T, 4.2 K) and $F_{p,max}$ values derived from our examination of the present wires. We have again used a value of $\lambda = 0.5$ as being appropriate for long laminar precipitates. Values of Q_{ppt} ($= F_p / \lambda l_{ppt}$), where l_{ppt} is the length of precipitate per unit area in transverse cross-section, are seen to range from 170 to 260 N/m². There is a general tendency for Q to decline with declining precipitate thickness; however, we do not understand the errors in our precipitate line length measurements and the choice of efficiency factor well enough to be sure whether the differences seen are significant or not. The low value of precipitate line length for the smallest wire is perhaps due to the disappearance of many ribbons below our measurement limit; this would produce an enlarged value of Q_{ppt} , as is indeed seen. It is interesting to note that the thickest precipitates (2.1 nm) have a Q_{ppt} value of 260 N/m², a value close to the Q_{gb} value previously measured (~ 300 N/m²) for the 2–3 nm thick grain boundary film.

The present results suggest that the production of thin (i.e. $\ll \xi$) normal precipitates is not in itself detrimental to the production of high pinning forces. The marked decrease in pinning predicted by the Kramer and Freyhardt [9] model seems not to be well-founded, as has been argued by Matsushita [10]. An alternative pinning mechanism that may be operating is that of quasi-particle scattering at the

precipitate–matrix interface [21]. A brief discussion applying this model to pinning in Nb–46.5 wt% Ti has been given by Somerkoski *et al.* [22]. These latter authors, however, consider sub-band boundaries to be the dominant pinning centers. We have argued against such an interpretation in an earlier paper [4], however, this scattering mechanism can certainly apply to both types of defect. More definitive experiments are needed to clearly elucidate the pinning in this complex system.

5.3. Intrinsic vs extrinsic properties

The quantitative description of the microstructure that we have presented here should in principle be suitable as the starting point for a discussion of the intrinsic flux pinning properties of the microstructure. The conclusion of recent discussions [7, 23–27] is, however, that we cannot simply assume that measurements of I_c , even at high sensitivity, yield a J_c which is characteristic of the local microstructural critical current density (J_{cm}), when the conversion factor of I_c to J_{cm} is the average cross-sectional area of the filaments. The evidence of Figs 10 and 13 shows that the filament quality (i.e. the lengthwise uniformity of the filament cross-section and/or its local J_{cm}) is declining, as the wire is drawn to its maximum J_c . The results shown in Figs 10 and 13 are believed to be rather typical of good composites. Thus, one can say rather generally that optimization of the J_c of a multifilamentary composite involves drawing it to the point at which an extrinsic limit due to filament sausageing is imposed on the J_c . Only in special cases, as for example when the large monofilaments are studied [29], is this not the case. In the present case, we note that the maximum J_c (5 T) was obtained when the relative standard deviation (σ_{n-1}/\bar{A}) of the filament cross-sectional area (A) was 8%, this rising to more than 12% at smaller sizes.

The connection between J_c and J_{cm} is not simple to make [26]. A first estimate can be made by increasing J_c by a factor accounting for the reduction of local area cross-section in a necked region. This would neglect any change produced by local microstructural changes (e.g. thinner and more closely spaced precipitates). Whatever the exact quantitative result, the net effect of these considerations is to suggest that the true local J_c (i.e. J_{cm}) continues to increase beyond the peak observed experimentally. The dashed line in the J_c plot in Fig. 14 illustrates our belief that the local current density continues to increase as the wire is drawn to smaller sizes. The dashed line in the precipitate thickness plot also indicates our belief that the wire thickness continues to decline. Thus precipitates thinner than 1 nm must be considered to be optimum for flux pinning for this composite. The magnitude of the difference between J_c and J_{ci} is presently being addressed by various experiments, including those which utilize an analysis of the critical current distri-

bution derived from an analysis of the resistive transition [23–28].

These comments suggest that some caution is needed in considering the change in shape of the F_p plots of Fig. 12 as being due to local microstructural changes. Warnes and Larbalestier [25, 26] have shown that the result of having a low n value is to make the ratio of the measured critical current, I_c (10^{-14} μm), to the average critical current, $\langle I_c \rangle$, diminish. When n is of order 70, this ratio is ~ 0.98 but this falls to ~ 0.93 when n is 30. These latter two values of n are characteristics of the largest and smallest wires examined here. We believe that the ratio of $\langle J_{cm} \rangle$ to $\langle I_c \rangle$ changes by a considerably greater amount however [26]. It thus seems appropriate to defer further discussion of the pinning force curve shape changes until we are more clear on these points.

6. CONCLUSION

1. Up to 20 vol.% of α -Ti was produced by multiple heat treatment. The optimum final drawing step was found to produce α -Ti precipitates < 1 nm thick, separated by 4 nm.

2. The optimum transport current density was found for precipitates whose thickness was about one fifth of a coherence length and whose separation was less than a coherence length.

3. The specific pinning force of 1–2 nm thick precipitates was found to be similar to grain boundary Ti-rich films of 2–4 nm thickness.

4. The optimum pinning forces observed in this composite are believed to have been limited by filament sausageing, suggesting that higher local J_c values would be found for even thinner, more closely spaced precipitates. No major evidence of proximity effect suppression of the pinning force was observed.

Acknowledgements—Discussions of various points with many members of the group are gratefully acknowledged; in particular, we thank Mary Buckett, Manfred Daeumling, Jim McKinnell, Christoph Meingast and Bill Warnes. Excellent experimental assistance in composite fabrication was provided by Scott Kreilick and Bill Starch. We thank W. K. McDonald and P. M. O'Larey of Teledyne Wah Chang for the supply of raw material and its chemical analysis. The work was supported by the Department of Energy, Division of High Energy Physics.

REFERENCES

1. A. W. West and D. C. Larbalestier, *Adv. Cryogenic Engng.* **26**, 471 (1980).
2. A. W. West and D. C. Larbalestier, *I.E.E.E. Trans. MAG.* **17**, 65 (1981).
3. A. W. West and D. C. Larbalestier, *Metall. Trans. A* **15**, 843 (1984).
4. D. C. Larbalestier and A. W. West, *Acta metall.* **32**, 1871 (1984).
5. A. W. West and D. C. Larbalestier, *I.E.E.E. Trans. MAG.* **19**, 548 (1983).
6. A. W. West, W. H. Warnes, D. L. Moffat and D. C. Larbalestier, *I.E.E.E. Trans. MAG.* **19**, 749 (1983).
7. D. C. Larbalestier, A. W. West, W. Starch, W. Warnes, P. J. Lee, W. K. McDonald, P. O'Larey, K. Hemachalem, B. Zeitlin, R. Scanlan and C. Taylor, *I.E.E.E. Trans. MAG.* **21**, 269 (1985).
8. D. C. Larbalestier and A. W. West, *Ann. Chimie. Sci. Materiaux* **9**, 813 (1984).
9. E. J. Kramer and H. C. Freyhardt, *J. appl. Phys.* **51**, 4930 (1980).
10. T. Matsushita, *J. appl. Phys.* **54**, 281 (1983).
11. T. S. Hutchison, G. Ocampo and G. J. C. Carpenter, *Scripta metall* **19**, 635 (1985).
12. M. J. Buckett and D. C. Larbalestier, *I.E.E.E. Trans. MAG.* **23**, (1987).
13. T. E. Cordier and W. K. McDonald, *I.E.E.E. Trans. MAG.* **11**, 280 (1975).
14. H. Hillman, in *Superconductor Materials Science* (edited by S. Foner and B. B. Schwartz), p. 275. Plenum Press, New York (1983).
15. D. C. Larbalestier, P. J. Lee and R. W. Samuel, *Adv. Cryogenic Engng.* **32**, 715 (1986).
16. M. Hansen and K. Anderko, *Constitution of Binary Alloys*, p. 1023. McGraw-Hill, New York (1958).
17. H. Hillmann, in *Superconductor Materials Science* (edited by S. Foner and B. B. Schwartz), p. 275. Plenum Press, New York (1982).
18. Y. Kouh Simpson, C. B. Carter, K. J. Merrissey, P. Angelini and J. Bentley, *J. Mater. Sci.* **21**, 2689 (1986).
19. E. J. Kramer, *Adv. Cryogenic Engng.* **28**, 307 (1982).
20. W. Yetter and E. J. Kramer, *J. Mater. Sci.* **17**, 2792 (1982).
21. E. V. Thuneberg, J. Kurkijarvi and D. Rainer, *Phys. Rev. B* **29**, 3913 (1984).
22. J. V. A. Somerkoski, E. V. Thuneberg and V. K. Lindroos, in *International Symposium on Flux Pinning and Electromagnetic Properties in Superconductors* (edited by T. Matsushita, K. Yamafuji and F. Irie), p. 106. Matsakuma Press, Fukuoka, Japan (1985).
23. W. H. Warnes and D. C. Larbalestier, *ibid.*, Ref. [22], 156.
24. W. H. Warnes and D. C. Larbalestier, *Appl. Phys. Lett.*, **48**, 1403, (1986).
25. W. H. Warnes and D. C. Larbalestier, *Cryogenics* (1986). To be published.
26. W. H. Warnes and D. C. Larbalestier, *I.E.E.E. Trans. MAG* **23**, (1987). To be published.
27. C. J. G. Plummer and J. E. Evetts, *I.E.E.E. Trans. MAG.* **32**, (1987).
28. D. P. Hampshire, H. Jones, *Proc. 9th Natn. Conf. on Magnet Technology* (edited by C. Marinucci), p. 453, Swiss Inst. Nuclear Research (1986).